Impregnation of Compressible Fiber Mats with a Thermoplastic Resin. Part I: Theory

V. MICHAUD AND J.-A. E. MÅNSON*
Laboratoire de Technologie des Composites et Polymères (LTC),
Ecole Polytechnique Fédérale de Lausanne (EPFL),
CH 1015 Lausanne, Switzerland

(Received March 14, 2000)
(Revised September 2, 2000)

ABSTRACT: In many cases of composite processing by liquid matrix impregnation, the fiber reinforcement is compressed when it comes in contact with the liquid and then relaxes as the matrix flows within its pores. This phenomenon can be analyzed in terms of local fluid flow, mass conservation and mechanical equilibrium. A model is proposed to simulate the kinetics of impregnation, and the evolution of the fiber volume fraction profile as the resin front progresses, as well as after the front has reached the end of the mold. The analysis is then applied to the case of infiltration of needled glass fiber preforms by a polypropylene matrix, used in the production of Glass Mat Thermoplastic blanks. A quantification of the effects of applied pressure and fluid viscosity on total process time is provided. It is shown that the time for preform relaxation after the fluid has filled the preform may be much larger than that for impregnation. As a result, an apparently well impregnated part may exhibit an inhomogeneous distribution of the reinforcement, in turn inducing a modification of the mechanical behavior and residual stress distribution.

KEY WORDS: liquid composite molding, thermoplastic composite processing, compressible porous media, glass mat thermoplastics.

INTRODUCTION

IN MOST COMPOSITE processing techniques, the resin in liquid form (molten thermoplastic or still uncured thermoset) must penetrate into a fiber assembly in order to produce a sound material. Matrix and reinforcement sizings are generally designed to enhance the thermodynamic capillary forces, so that spontaneous infiltration could be expected. In practical cases, however, external pressure must be

*Author to whom correspondence should be addressed.

1530-793X/01/13 1150–24 $10.00/0 DOI:10.1106/8108-1VMC-B4FG-FXPU

Journal Online at http://techpub.metapress.com

applied on the polymer to speed up the process, in particular with resins of high viscosity. The applied pressure is transmitted to the preform assembly, which may thus deform during impregnation, thereby altering the kinetics of the process and the homogeneity of the final part. Since fiber preforms used in the processing of composite materials are rather compliant porous materials [1,2], significant preform deformation has been reported in most cases of composite processing [1–6]. Models have been proposed to describe the behavior of fiber mats in compression [1,7], which have been confronted to experimental stress-strain curves obtained for a range of preform types [8]. The relaxation of preforms after compression is often observed to differ from the behavior in compression, the hysteresis being attributed to fiber sliding and rearrangement or breakage [4,9]. As preform compression was recognized to play a large role in compression modeling or autoclave curing of already impregnated fiber beds, a number of models have been developed to describe the compression of an already impregnated preform with lateral flow of fluid being squeezed out [1,10,11]. The recent interest in injection-compression liquid composite modeling has also led to the development of models taking into account the compression of the impregnated assembly [12,13]. Preform compressive behavior is less often taken into account in other types of composite processing whereby the liquid resin impregnates a dry preform, such as RTM or thermoplastic impregnation including film stacking within a closed mold. In such cases, the liquid resin first compresses the preform, which subsequently relaxes as the fluid penetrates the dry preform. As the process occurs in a closed mold, no lateral flow is allowed, and both matrix and preform withstand the externally applied pressure. Simultaneous fluid flow and mechanical equilibrium thus need to be taken into account. The phenomenon of fluid flow within deformable porous media being encountered in many other branches of engineering such as soil science or biomechanics, methods derived in these fields have been successfully applied in composite processing studies, and are reviewed in References [14,15]. In particular, Sommer et al. [14] recently proposed a treatment of infiltration of initially dry deformable porous media, based on a soil mechanics approach. This treatment neglects inertial forces as well as thermal and chemical transport phenomena, and uses the slug-flow assumption, which makes all infiltration take place along a two-dimensional front within the preform. This analysis was implemented fully for infiltration in one direction under constant applied pressure using the Boltzmann transformation to reduce the variables' position and time into a combined variable, and was validated using experiments on the infiltration of a polyurethane sponge by ethylene glycol. The method was further extended to the case of non-isothermal infiltration of a porous preform by molten metal, taking into account solid phase formation [9]. An analysis along similar lines by Preziosi and co-workers [16,17] provided a theoretical evaluation of the effects of inertial forces and of various constitutive equations for the stress term for infiltration of a dry porous preform and for relaxation of an initially compressed wet porous me-

dium. Recently, Antonelli et al. used a similar approach to propose a model for RTM, but no experimental results are provided for validation [18].

In this paper, we propose to extend the method developed in Reference [14] to practical cases of thermoplastic polymer composite impregnation processes. A model is proposed to predict the kinetics of impregnation and the evolution of the fiber volume fraction distribution during impregnation, as well as after the front has reached the end of the mold, as the fiber bed relaxes within the fluid. The analysis is then applied to a case of practical interest, the impregnation of needled glass fiber mats by polypropylene for the manufacturing of Glass Mat Thermoplastic (GMT) blanks.

GENERAL STATEMENT OF THE PROBLEM

We consider the isothermal infiltration in one direction of an initially dry fiber preform by molten polymer under constant applied pressure P_a, exerted by a piston, as described schematically in Figure 1(a) and (b) for two cases treated in this article. For both cases, we assume that infiltration takes place in a closed mold, so that one end and the sides of the preform are restrained by the mold walls. We neglect any lateral friction between the mold walls and the sides of the preform. Both flow and strain are assumed to take place along the x-direction only. Capillary forces are neglected at the infiltration front, because these are generally low in polymer infiltration compared to the level of applied pressure. A constant capillary pressure drop at the infiltration front could however easily be included as in References [9,14]. The pressure at the infiltration front is thus exactly the gas pressure at that location, P_g, assumed to remain constant due to the presence of an air path in the mold. We assimilate the porous medium to a continuum, and define the local fiber volume fraction as V_f. We neglect all body forces and inertial forces, and assume for simplicity the matrix behavior to be Newtonian, so that Darcy's law is valid. We further assume that the porous medium is isotropic in a plane perpendicular to the x-axis, such that the infiltration direction is a principal axis of the permeability tensor. In the first instant of pressure application, the liquid is decelerated by the porous preform during a transient period. Simultaneously, the preform is compressed to the volume fraction V_f^c corresponding to the applied pressure P_a. As in previous studies [9,14], we do not consider the dynamics of this transient phase. We thus simplify the problem by taking compression of the porous medium to be instantaneous. The position of the compressed preform entrance at $t = 0$ is defined as $x = 0$, and the x-axis remains fixed in relation to the mold wall, and oriented along the direction of infiltration. We also include in Figure 1 another system of axes marked as z, where $z = 0$ at the mold wall (corresponding to $x = x_m$) and oriented along the direction of preform relaxation, opposite to the direction of infiltration. The purpose of the z-axis is only to allow a more convenient representation of the relaxation results.

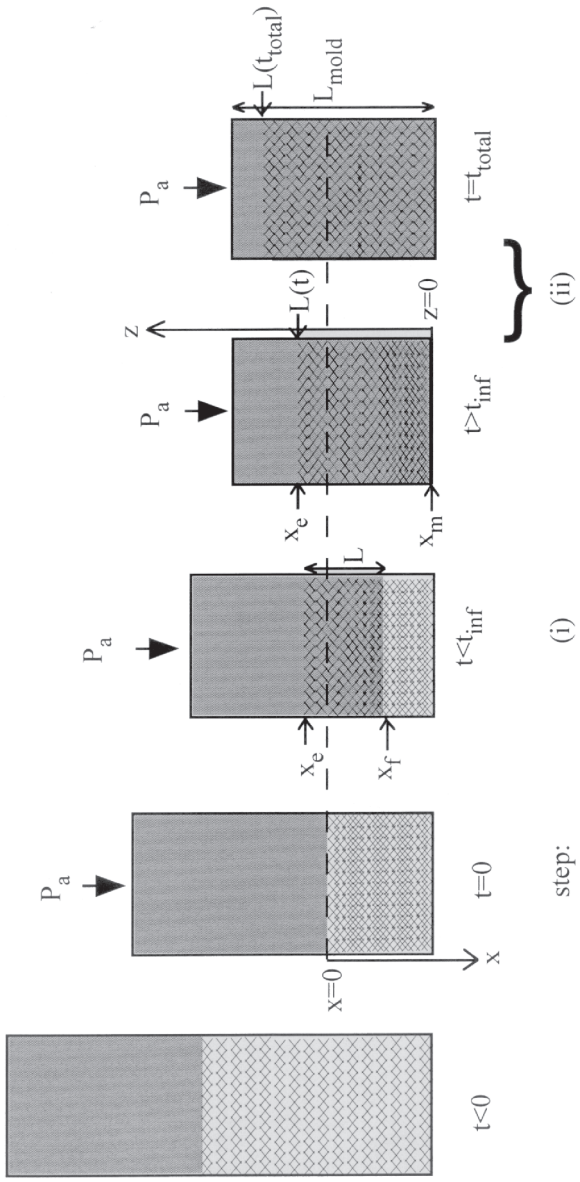

Figure 1. *Schematic description of the preform impregnation process: (a) represents the case where the amount of resin is large and the preform relaxes completely after infiltration, involving steps (i) and (ii) as described in the text; (b) represents the case where the preform reaches the other end of the mold before relaxing completely, involving steps (i), (ii) and (iii). The z-axis marked in this figure is used as the reference axis in Figures 6(a), 7 and 8(a).*

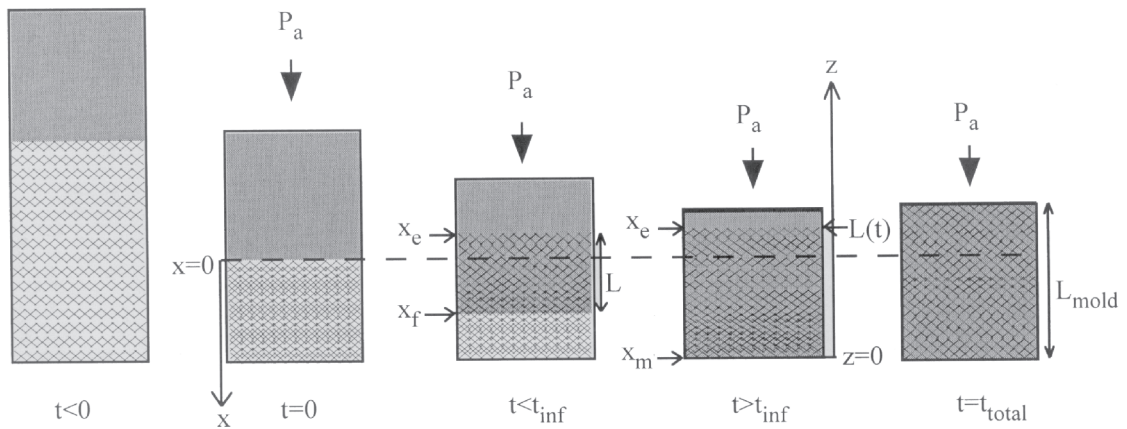

(b)

Figure 1 (continued). *Schematic description of the preform impregnation process: (a) represents the case where the amount of resin is large and the preform relaxes completely after infiltration, involving steps (i) and (ii) as described in the text; (b) represents the case where the preform reaches the other end of the mold before relaxing completely, involving steps (i), (ii) and (iii). The z-axis marked in this figure is used as the reference axis in Figures 6(a), 7 and 8(a).*

In a first step (i), marked in Figure 1(a) and (b), as infiltration of the dry preform proceeds, the local pressure P in the liquid increases from P_g behind the infiltration front to $P_a + P_g$ at the preform entrance. Infiltration is supposed to occur in a slug-flow manner, such that there is a sharp infiltration front between the dry preform and the fully infiltrated preform containing no residual porosity. The preform accordingly relaxes behind the infiltration front, along the stress-strain curve of the preform in relaxation. When the polymer has traveled across the preform thickness to the mold wall, at $t = t_{inf}$, infiltration is complete. During a second step (ii), the preform then relaxes further within the liquid. The preform eventually reaches a fully relaxed state, $V_f = V_f^r$ as shown in Figure 1(a). If the preform has reached the other end of the mold before being completely relaxed, as shown in Figure 1(b), a final step (iii) occurs, in which the remaining gradients in volume fraction smooth out to reach an equilibrium volume fraction which is higher than the value in the relaxed state.

GOVERNING EQUATIONS

The governing equations are written in one dimension over a representative volume element ΔV, following Reference [14]. Darcy's law is written as:

$$u_l - u_s = -\frac{K}{\eta(1-V_f)}\frac{\partial P}{\partial x} \tag{1}$$

where u_l is the (positive) average local velocity of the liquid within the pores, u_s the (negative) local velocity of the solid, K (a function of V_f) is the permeability of the porous medium in ΔV, η is the liquid viscosity, and P is the pressure in the liquid.

Mass conservation in the solid and liquid phases, respectively, dictates:

$$\frac{\partial V_f}{\partial t} + \frac{\partial (V_f u_s)}{\partial x} = 0 \tag{2}$$

and

$$-\frac{\partial V_f}{\partial t} + \frac{\partial ((1-V_f)u_l)}{\partial x} = 0 \tag{3}$$

Finally, having neglected inertial and body forces in both solid and liquid, stress equilibrium implies:

$$\frac{\partial P}{\partial x} = -\frac{\partial \sigma}{\partial x} \tag{4}$$

where σ is the effective stress acting in the solid along x, counted as positive in compression and averaged over a surface area comprising both solid and liquid.

The boundary conditions are written for the two or three steps defined earlier which determine the process. In the first step (i), an initially dry porous medium is infiltrated by polymer. Thus, at the infiltration front $x = x_f(t)$, $V_f = V_f^c$, $P = P_g$ which is constant assuming that the gas can escape through the mold ahead of the infiltration front, and $u_s = 0$. At the preform entrance $x = x_e(t)$, $P = P_a + P_g$ and $V_f = V_f^r$. In the second step (ii), the polymer has reached the end of the mold and the preform relaxes. Therefore, at the front, which is the mold wall position, $x = x_m$, $u_s = u_l = 0$. At the preform entrance, $x = x_e(t)$, $V_f = V_f^r$. If the mold has a size smaller than the relaxed length of the preform, the preform entrance will reach the mold wall before complete relaxation. The third step (iii) is then encountered, with $x_e(t)$ = constant = $x_m - L_{mold}$, where L_{mold} is the total length of the mold, dictated by the initial volumes of fiber and polymer, assuming no residual porosity.

SOLUTION METHODOLOGY

Due to the different boundary conditions, the equations governing each step are solved separately, the results of step (i) being implemented as initial volume fraction distribution in the solution of step (ii), and the results of step (ii) after the preform reaches the other end of the mold are implemented if necessary as initial volume fraction distribution in step (iii).

Solution for Step (i)

As the applied pressure is constant, step (i) is solved following the methodology proposed in Reference [14], using the Boltzmann transformation to define a reduced parameter, χ as

$$\chi = \frac{(x - x_e)}{\psi\sqrt{t}} \tag{5}$$

where ψ is chosen such that $L(t) = x_f - x_e = \psi\sqrt{t}$.

The functions $l(\chi)$ and $s(\chi)$ are defined by:

$$u_l = \frac{\psi\, l(\chi)}{2\sqrt{t}} \tag{6}$$

$$u_s = \frac{\psi\, s(\chi)}{2\sqrt{t}} \tag{7}$$

Using this transformation, Equations (1) to (4) become a set of nonlinear ordi-

nary first-order differential equations of the three functions V_f, l and s:

$$V_f' = \frac{(l-s)(1-V_f)\eta\psi^2}{2K(V_f)\dfrac{\partial\sigma}{\partial V_f}} \tag{8}$$

$$s' = [s - \chi - s(0)]\left(\frac{-V_f'}{V_f}\right) \tag{9}$$

$$l' = [l - \chi - s(0)]\left(\frac{V_f'}{1-V_f}\right) \tag{10}$$

where prime denotes derivation with respect to χ. The sum of Equations (9) and (10) additionally yields:

$$((1-V_f)l + V_f s)' = 0 \tag{11}$$

s and l are therefore always linked, and the value of the average velocity: $((1 - V_f)1 + V_f s)$ is dictated by the values at $\chi = 1^-$ and at $\chi = 0$.

Considering the boundary conditions, as described in Reference [14]:

$$V_f = V_f^c \text{ at } \chi = 1^- \tag{12}$$

$$V_f = V_f^r \text{ at } \chi = 0 \tag{13}$$

$$s(\chi = 1^-) = 0 \tag{14}$$

and

$$l(\chi = 1^-) = 1 + s(0) \tag{15}$$

the entire problem can be solved for the two functions s and V_f only, with 1 deduced from the solution as

$$l(\chi) = \frac{(1-V_f^c)(1+s(0)) - V_f(\chi)s(\chi)}{(1-V_f(\chi))} \tag{16}$$

The set of 2 nonlinear first-order equations defined by Equations (8) and (9) is solved numerically using Mathematica™ for the parameter ψ and the functions $V_f(\chi)$ and $s(\chi)$, using a numerical integration scheme and a two-dimensional Newton-Raphson method to adjust the initial guesses of ψ^2, and $s(\chi = 0)$ for convergence. The time at which the infiltration front reaches the end of the preform is then obtained as:

$$t_{\text{inf}} = \frac{x_m^2}{\psi^2(1 + s(0))^2} \tag{17}$$

where x_m is the height of the preform at $t = 0$, when compressed to $V_f = V_f^c$.

Simplified solution: $(-u_s) \ll u_l$. A simplified solution obtained by neglecting the solid phase velocity as compared to the liquid phase velocity was proposed and validated in Reference [14] and used as well in Reference [9]. The infiltration rate parameter ψ is in this case directly obtained by setting $V_f = V_f^r$ at $\chi = 0$ in the following equation (derived as in Reference [14]):

$$\int_{V_f(\chi)}^{V_f^c} 2K(V_f)\sigma'(V_f)dV_f = (1 - V_f^c)\eta\psi^2(1 - \chi) \tag{18}$$

and solving for ψ. The volume fraction V_f and the effective stress σ can then be calculated as functions of χ by solving Equation (18) again, but for arbitrary χ. Even if this solution is not valid in many cases of highly compressible preforms, it allows a quick estimate of the parameter ψ which can then be introduced as a first guess in the numerical solution procedure.

Solution for Step (ii)

In step (ii), as the value of V_f at $x = x_m$ decreases with time, no similarity solution can be used, and the variables x and t will be considered. The sum of Equations (2) and (3), associated with the boundary condition that $u_s = u_l = 0$ at $x = x_m$, indicates that

$$(1 - V_f)u_l + V_f u_s = 0 \tag{19}$$

This result is the same as Equation (11), with the additional condition that this average velocity is 0. Combining with Equations (1) and (4), the resulting equation to solve is:

$$\frac{\partial V_f}{\partial t} + \frac{\partial}{\partial x}\left(D(V_f)\frac{\partial V_f}{\partial x}\right) = 0 \tag{20}$$

where

$$D(V_f) = -V_f \frac{K(V_f)}{\eta} \frac{d\sigma}{dV_f} \tag{21}$$

The position of the moving front, $x = x_e(t)$, where $V_f = V_f^r$, is found by Equation (1), written as:

$$\frac{dx_e}{dt} = u_s \Big|_{x=x_e} = -\frac{K(V_f)}{\eta} \frac{d\sigma}{dV_f} \frac{\partial V_f}{\partial x} \Bigg|_{x=x_e} \tag{22}$$

or alternatively by using a macroscopic mass conservation equation for the solid phase.

The set of equations is solved with an explicit finite difference scheme, forward in time, centered in space, as used for such non-linear diffusion type problems [19]. The initial distribution of V_f for this step is taken as the result $V_f(\chi)$ for step (i) at $t = t_{inf}$ defined in Equation (17), discretized according to the number of grid points. Since one boundary is moving ($x = x_e(t)$), a change of variable is operated, by defining $\xi(x,t) = x/[x_e(t)]$. Differentiation is thus performed along a moving grid, but the number of grid elements and the grid spacing remain constant at each step, in terms of ξ, using a method proposed in References [19–21]. At each time step, the new position of x_e is evaluated by a global mass conservation. The numerical integration code was written in FORTRAN, the number of time steps being imposed by the stability criterion $(2D\Delta t)/\Delta x^2 \leq 1$, where Δt is the time step and Δx the grid spacing. As Δx increases with time, provided that $D(V_f)$ does not change much, the time step can also be increased at each step to speed up the calculation while preserving the stability of the solution. The code was validated using the example of the relaxation of a polyurethane sponge in ethylene glycol initially compressed to a constant volume fraction using experimental system parameters determined in Reference [14]. The numerical results were in good agreement with those obtained by Preziosi and co-workers treating this similar problem with a slightly different numerical approach [15].

Solution for Step (iii)

In step (iii), the set of equations becomes a non-linear diffusion type of problem, with no moving boundary, as $x_e(t) = \text{constant} = x_m - L_{mold}$. Equation (20) is thus solved by finite difference as in step (ii) with a fixed grid. The initial distribution of V_f for this step is taken as the final distribution given from step (ii) at the time t_{relax} when $x_e(t_{relax}) = x_m - L_{mold}$. The calculation is stopped at $t = t_{equil}$ when the gradient in fiber volume fraction is less than a given tolerance value (typically 10% variation between x_m and x_e in our calculations).

RESULTS AND DISCUSSION

As a practical application of the present analysis, we consider the unidirectional infiltration under constant applied pressure of polymer into a needled glass fiber mat of initial volume fraction 4%. The mats consist of fiber bundles about 250 μm in diameter randomly distributed in a plane, with some fibers in the orthogonal plane resulting from the needling operation performed to confer some structural integrity to the porous fiber bed. The physical data for this system are based on experimental measurements and the reader is referred to References [22,23] for further details concerning the experimental procedures.

The permeability of the fiber mats, as a function of fiber volume fraction is taken as:

$$K = 3.4978 \cdot 10^{-31} (1 - V_f)^{10.743} \tag{23}$$

The relation between σ and V_f is obtained by a curve fit of experimental compression tests of sized fiber mats at various applied pressures, and is given as follows:

- for the compression part of the curve, with σ given in Pa:

$$\sigma = a_0 + a_1 V_f + a_2 V_f^2 + a_3 V_f^3 + a_4 V_f^4 \tag{24}$$

  with $a_0 = 1.1958 \cdot 10^5$, $a_1 = -4.8888 \cdot 10^6$, $a_2 = 6.7048 \cdot 10^7$, $a_3 = -3.5488 \cdot 10^8$, $a_4 = 7.0216 \cdot 10^8$
- for the relaxation part of the curve, with σ given in Pa:

$$\sigma = \sigma_c (m_0 + m_1 a + m_2 a^2 + m_3 a^3 + m_4 a^4) \tag{25}$$

  where

$$a = \left(\frac{V_f^c + 0.0001 - V_f}{V_f^c + 0.0001 - V_f^r} \right)^{1/3} \tag{26}$$

  σ_c is the compression stress before relaxation, V_f^c is the fiber volume fraction at σ_c obtained from Equation (24), V_f^r is the fiber volume fraction at σ = 0, taken as $V_f^r = 0.06$, and $m_0 = 1.102025$, $m_1 = -1.0222325$, $m_2 = -4.197025$, $m_3 = 7.300125$, $m_4 = -3.18695$. The resulting shape of the curve is given in Figure 2. The influence of lubrication and strain rate being minimal for this type of preform [22], the relaxation part of the curve should thus accurately represent the intrinsic behavior of the preform relaxation during the process.

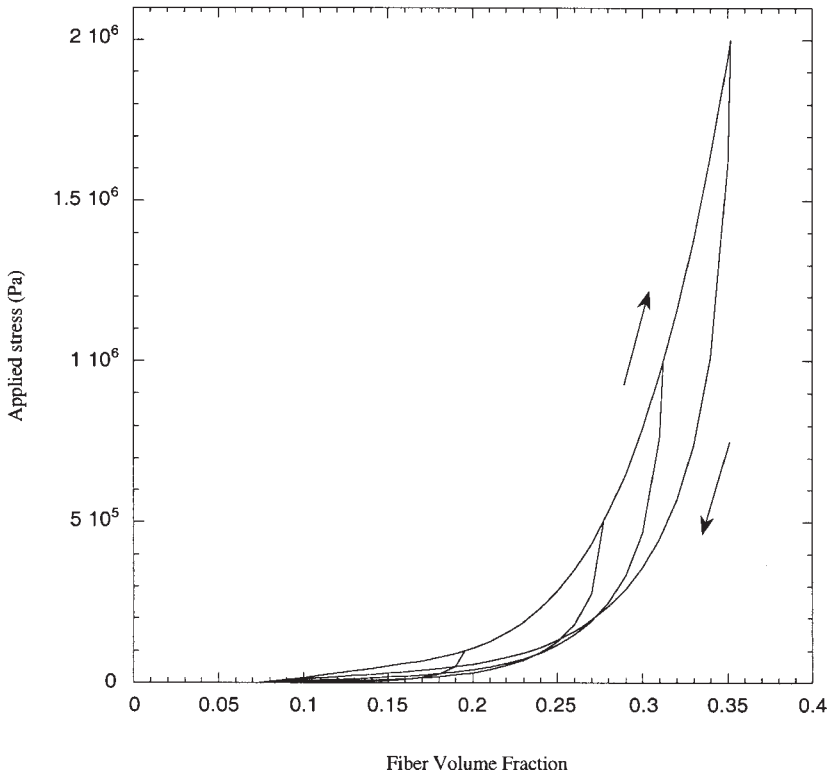

Figure 2. *Stress-strain curve for the glass fiber preform at 4 different compression levels.*

The viscosity η of the polymer is taken as a constant, most of the calculations being performed with a representative value taken as $\eta = 250$ Pa·s unless specified otherwise, corresponding to a typical value for polypropylene at 200°C.

In a typical model experiment, two mats are stacked in a mold, so that the initial preform thickness is 11.3 mm for a fiber volume fraction of 4%. A layer of polypropylene is placed on top, and impregnation is performed under constant pressure P_a applied by a piston. Two cases are considered: if the initial thickness of polypropylene is greater than the relaxed preform thickness divided by $(1 - V_f^r)$, i.e.,8 mm, the preform will relax completely and only steps (i) and (ii) will be considered. If the polymer thickness is less, the preform will not relax completely, and step (iii) will be considered as well. A typical case considered in what follows is $x_m - L_{mold} = 3.48$ mm, leading to a final average fiber volume fraction in the composite of 13%, corresponding to that of a typical GMT blank.

The kinetics of infiltration for step (i) are plotted in terms of ψ^2 as a function of

applied pressure in Figure 3 for various cases, considering (a) no compression of the preform at all, with $V_f = 0.04$ remaining constant, (b) no relaxation of the preform at all, with $V_f = V_f^c(P_a)$ remaining constant, as well as using the analysis described earlier with (c) the simplified solution given in Equation (18) and (d) the full numerical solution. It appears clearly that in the case of needled glass preforms, the preform infiltration kinetics cannot be accurately described without taking into account the preform compression and relaxation during the process. The simplified solution gives somewhat inaccurate results, with a deviation of about 10% at high pressures, but may provide a quick first estimate of the infiltration kinetics without the need of a numerical code. We observe that for the range of pressures considered here, the infiltration kinetics increase with applied pressure, indicating that the increase in infiltration driving force caused by the pressure gradient is not yet counterbalanced by the decrease in permeability, as was for example observed in Reference [9]. It is however expected that the infiltration kinetics

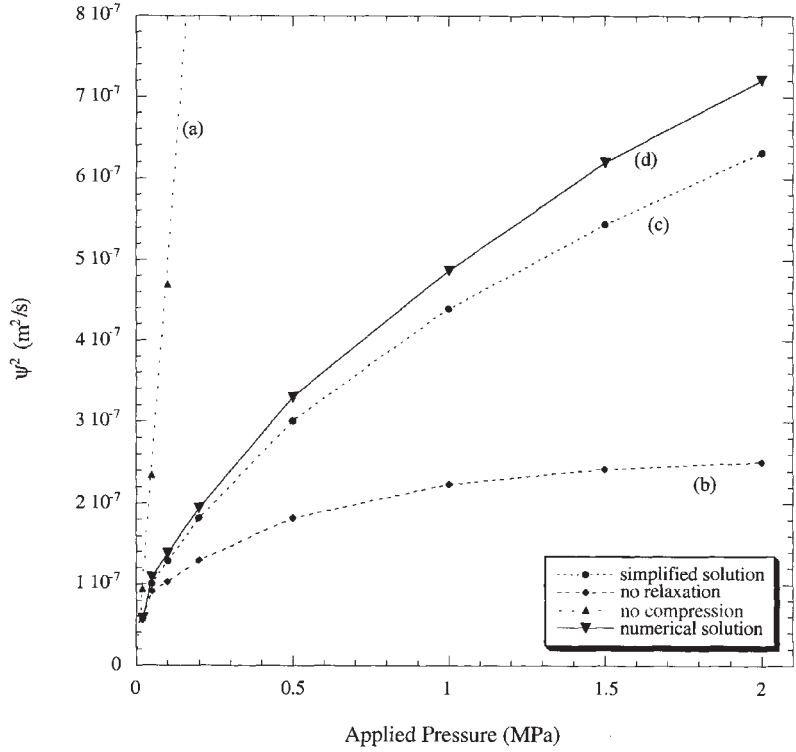

Figure 3. *Infiltration kinetics as a function of applied pressure, for 4 cases: (a) assuming no compression of the preform, (b) assuming no relaxation of the compressed preform, (c) assuming relaxation of the preform using the simplified solution and (d) assuming relaxation of the preform using the full numerical solution.*

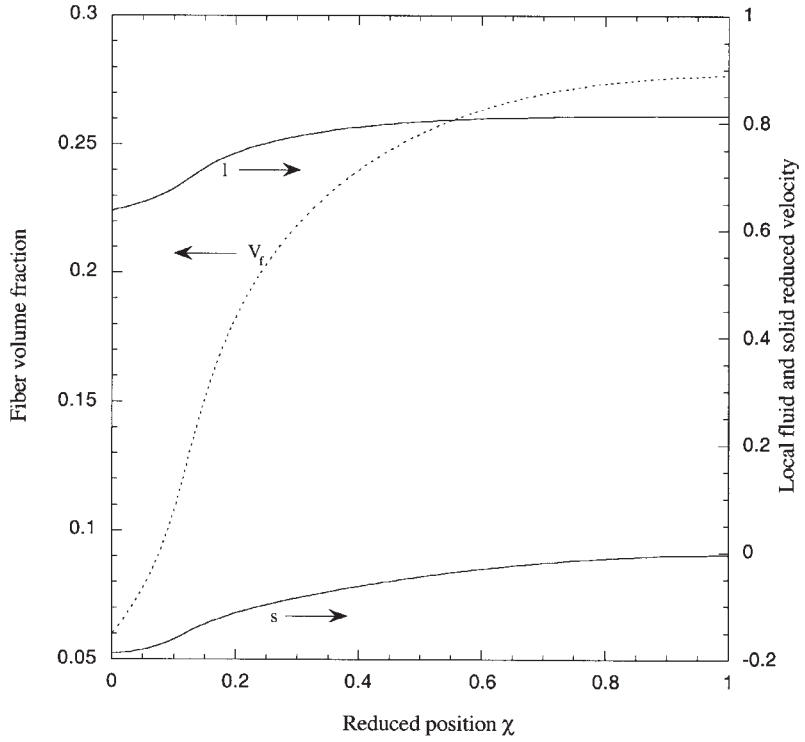

Figure 4. *Profiles of the fiber volume fraction, and the reduced fluid and solid velocities as a function of the reduced position* χ *for infiltration under an applied pressure of* $P_a = 0.5$ *MPa.*

should reach a plateau towards the high pressure range. An example of profiles of V_f, s and l solution of Equations (8,9,16) as a function of χ is given in Figure 4, for $P_a = 0.5$ MPa. A strong gradient in fiber volume fraction is observed along the length of the sample, the maximum value being $V_f^c = 27.5\%$ at the front, as observed in Figure 2. The variation in fluid and solid velocities is less drastic, and is given in Figure 5 in non-reduced coordinates for an infiltration time of $t = 10$ s. At that time, the fluid velocity is between 60 and 80 μm/s, justifying the assumption of laminar flow and Newtonian fluid taken in the analysis as the corresponding shear rates are low. The solid velocity is negative, since the solid phase moves back, with a maximal velocity of about −17 μm/s at the preform entrance. The value of the local pressure P in the fluid is evaluated considering the total force equilibrium: $P_a + P_g = \sigma(V_f) + P$, and is also plotted as a function of distance in Figure 5. The local pressure varies in opposition to the level of pressure borne by the fiber network from P_g at the infiltration front to $P_a + P_g$ at the preform entrance.

The fiber volume faction profiles as a function of distance for step (ii), after infiltration under P_a = 0.5 MPa are given in Figure (6a), for relaxation in an infinite mold, and the corresponding value of the preform length as a function of time is plotted in Figure 6(b). The initial profile is taken at t_{inf}, which in this case is 13 s. The initially very strong gradient is slowly reduced with time for relaxation within a polymer of such a viscosity (250 Pa·s). The time for full relaxation is above 2 hours, whereas the time for infiltration was 13 s, indicating that an apparently impregnated preform may exhibit very large gradients in reinforcement. Such a graph could be used for the manufacturing of graded composite materials, by providing a time at which to stop relaxation by quenching the sample, as an alternative to other more time consuming methods such as the one described in Reference [24].

If the polymer initial volume is adjusted to obtain a final fiber volume fraction

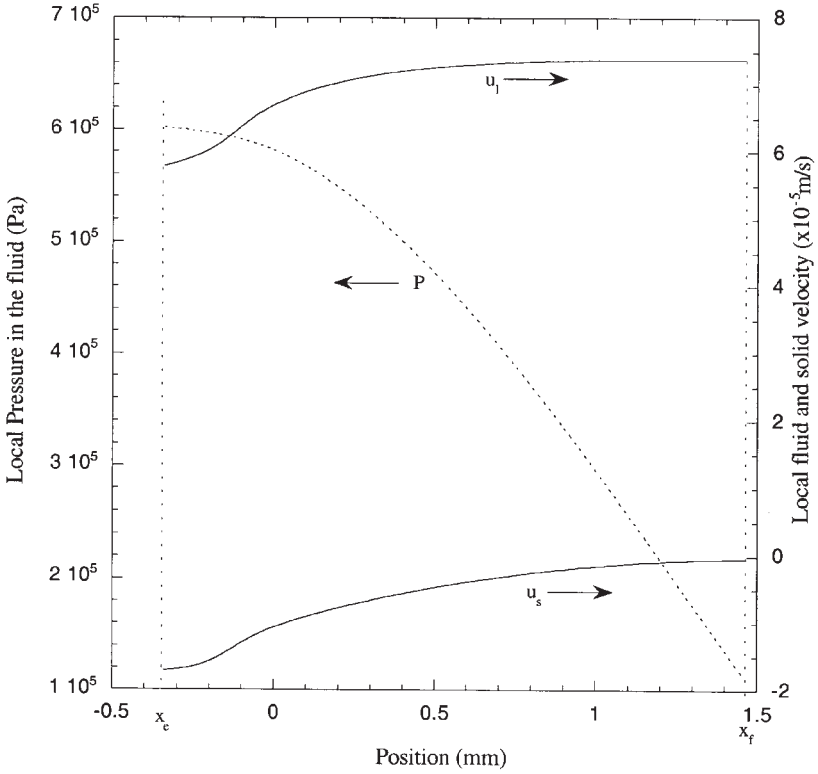

Figure 5. *Profiles of the local pressure in the fluid, and the local fluid and solid velocities as a function of position in the mold, for an infiltration time of 10 s, under an applied pressure of* P_a *= 0.5 MPa.*

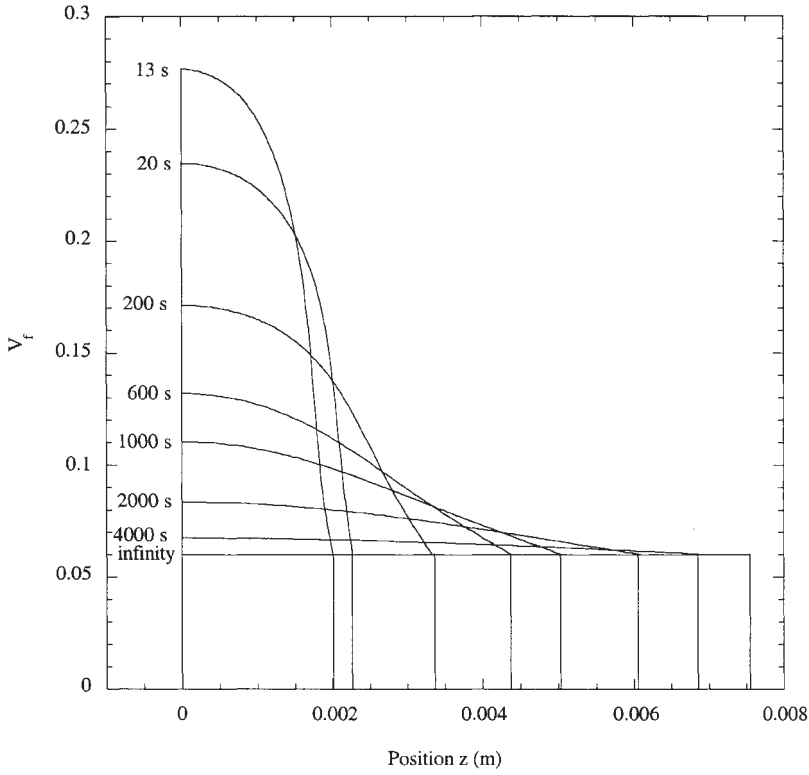

(a)

***Figure 6**. (a) Distribution of the volume fraction fiber as a function of position in the mold, after full impregnation under an applied pressure of P_a = 0.5 MPa, for various times from t_{inf} = 13 s to infinity and (b) evolution of the total preform length as a function of time, under the same conditions.*

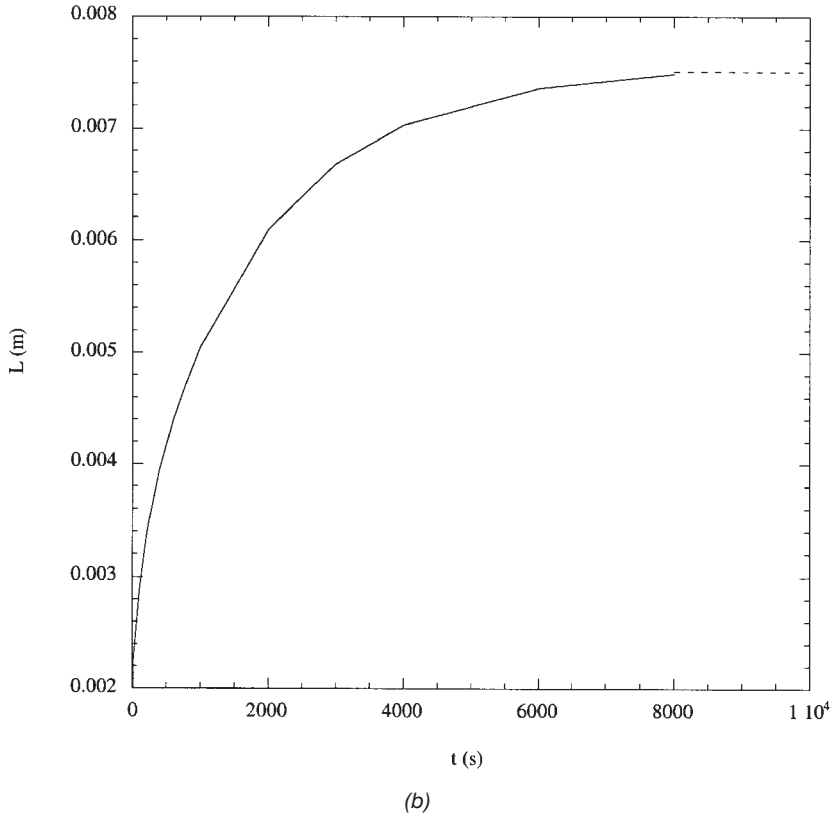

(b)

Figure 6 (continued). *(a) Distribution of the volume fraction fiber as a function of position in the mold, after full impregnation under an applied pressure of* $P_a = 0.5$ *MPa, for various times from* $t_{inf} = 13$ *s to infinity and (b) evolution of the total preform length as a function of time, under the same conditions.*

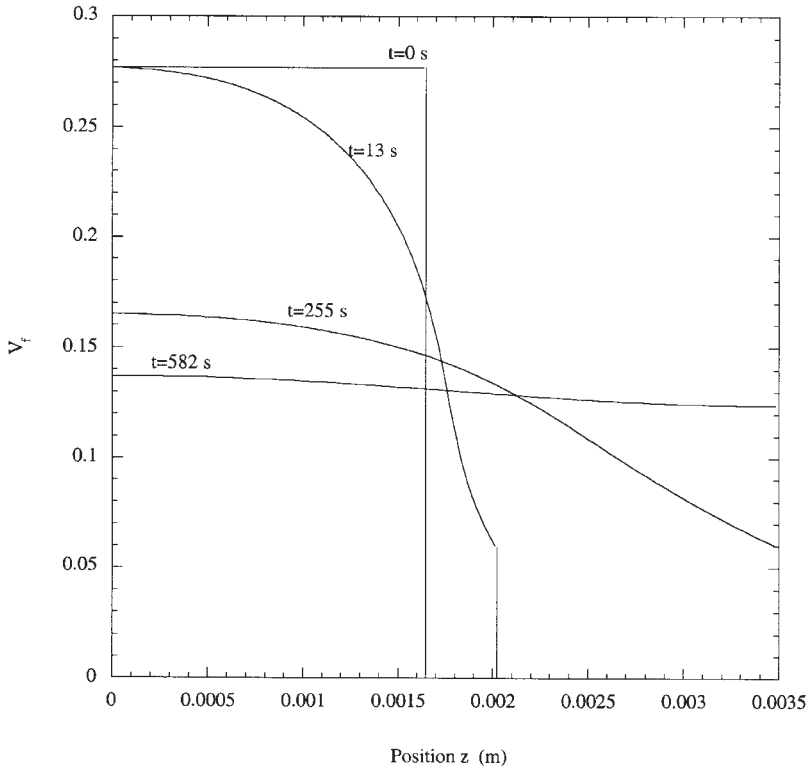

Figure 7. *Distribution of the volume fraction fiber as a function of position in the mold for the case of partial relaxation allowed, after infiltration under an applied pressure of* P_a *= 0.5 MPa, for various times corresponding to* $t = 0$, $t = t_{inf}$, $t = t_{inf} + t_{relax}$ *and* $t = t_{inf} + t_{relax} + t_{equil}$.

higher than V_f^r, the reinforcement profile evolves as shown in Figure 7, for $P_a = 0.5$ MPa. The preform reaches the other end of the mold at $t_{inf} + t_{relax} = 242$ s + 13 s = 255 s. V_f still varies between 16.5 and 6% across the thickness of the sample. The fiber volume fraction subsequently equilibrates, and reaches a uniform value around 13% (within 10% variation) after another $t_{equil} = 327$ s. The total time required to obtain a uniform sample is therefore $t_{total} = 582$ s, about 10 minutes. The corresponding plot of the local pressure in the fluid as a function of position using the z-axis as shown in Figure 1, taking 0 at the mold wall for the sake of clarity, is given in Figure 8(a) for various times. The local pressure at $x = L(t)$ is equal to $P_a + P_g$ during infiltration and relaxation, and then decreases during the equilibration period to reach an equilibrium value of $P_a + P_g - \sigma(V_{final})$. On the other side of the preform, near the mold wall, the local pressure slowly increases as

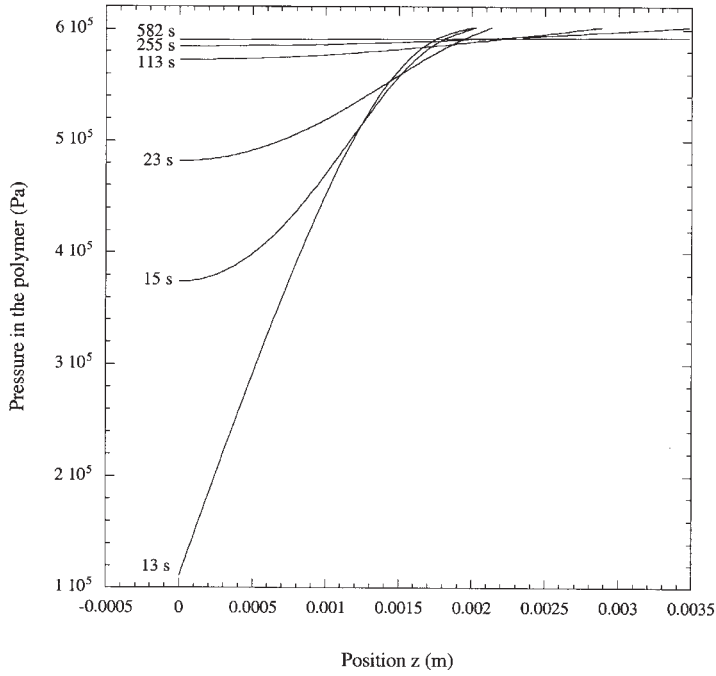

(a)

Figure 8. *(a) Local pressure in the fluid as a function of position in the mold and time for infiltration in the conditions corresponding to Figure 7 and (b) evolution of the local pressure in the polymer with time, for three locations within the preform, corresponding to near the mold wall ($x = x_m$), near the preform entrance ($x = x_e(t)$) and in between.*

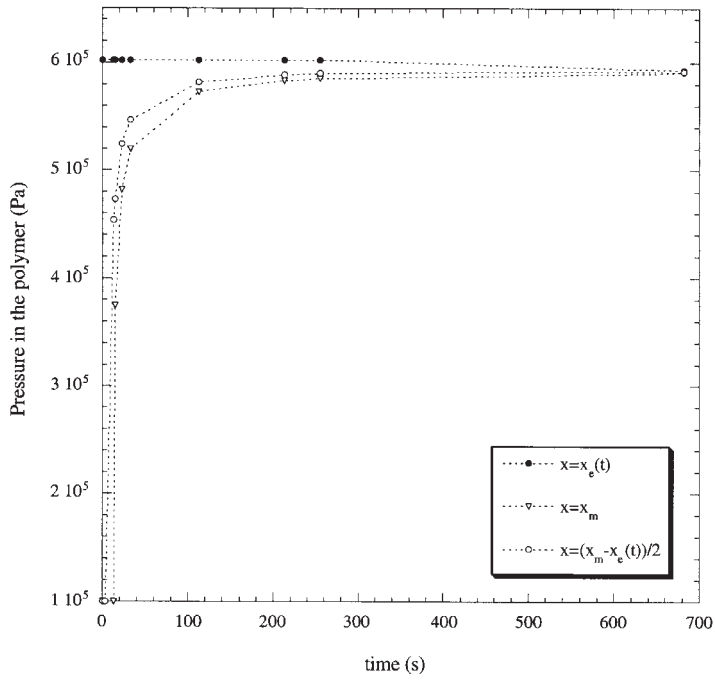

(b)

Figure 8 (continued). *(a) Local pressure in the fluid as a function of position in the mold and time for infiltration in the conditions corresponding to Figure 7 and (b) evolution of the local pressure in the polymer with time, for three locations within the preform, corresponding to near the mold wall ($x = x_m$), near the preform entrance ($x = x_e(t)$) and in between.*

the preform locally relaxes. The evolution of the local pressure in the fluid versus time, at three locations on the preform, namely $x = x_e(t)$, $x = (x_m - x_e)/2$ and $x = x_m$, is given in Figure 8(b). The slow raise of fluid pressure near the mold wall may have an impact on the quality of impregnation, particularly as will be discussed in Part II, if the fiber bundles are not fully impregnated during flow, and are subsequently filled by radial impregnation within the local pressure field. Also, it is important to note that if high volume fraction blanks, for example with $V_f = 25\%$, are to be produced by this method, the local pressure in the polymer at the end of the process will be $P_a + P_g - \sigma(V_{ffinal}) = 0.3$ MPa. As a result, near the preform entrance, the pressure in the polymer will decrease from 0.6 to 0.3 MPa during the process. This, in turn, may favor entrapped gas dissolution or deconsolidation within the bundles.

The influence of the polymer viscosity on the values of t_{inf}, t_{relax} and t_{equil} for an applied pressure of $P_a = 0.5$ MPa is given in Figure 9. As expected from the form of the equations, and as used in Reference [16], time in all the equations (1 to 4) could be replaced by a non-dimensional reduced time, by dividing t by η and x_m^2, and multiplying it by a representative value of $K(V_f)$ and $\sigma(V_f)$. The influ-

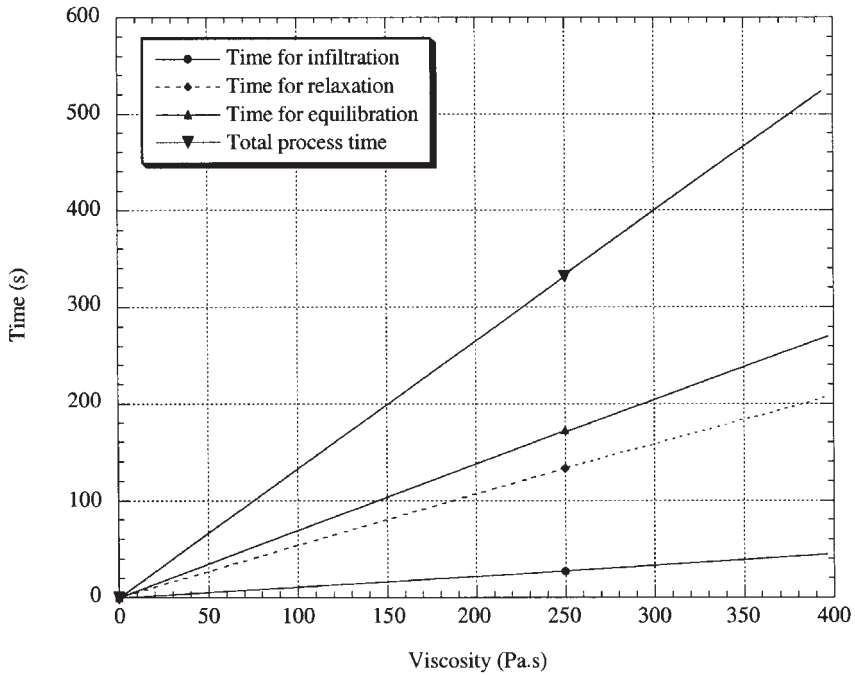

Figure 9. *Plot of the time for infiltration, time for relaxation, time for equilibration and total process time as a function of the fluid viscosity, for infiltration under an applied pressure of* $P_a = 0.5$ *MPa.*

ence of viscosity on all the calculated times is thus linear, and the influence of the initial preform thickness at a given applied pressure is quadratic. For a given viscosity and geometry, the influence of the applied pressure is much less intuitive, as shown in Figure 10. The time for infiltration decreases when the pressure increases, as was already noticed when considering the infiltration kinetics (Figure 3). Note that above 0.1 MPa, the time for infiltration becomes negligible compared that for the other steps. The time for relaxation and the time for equilibration, for the typical chosen geometry increases significantly with applied pressure. This can be related to the shape of the preform stress-strain curve (Figure 2); also, since relaxation is very slow in high viscosity liquids, it clearly becomes the limiting step. In summary, for the case considered here, the total time for producing a homogenous sample increases as the applied pressure increases. This indicates that process optimization would require using the lowest possible applied pressure, that is the pressure corresponding to the final volume fraction to be obtained, for example $P_a = 0.05$ MPa for our example of $V_{ffinal} = 13\%$.

This analysis applies to the case of completely saturated fluid flow. As will be discussed in the next publication [23], in the case of fiber bundle mat impregnation, the fluid may flow around the bundles first, leaving unimpregnated tows,

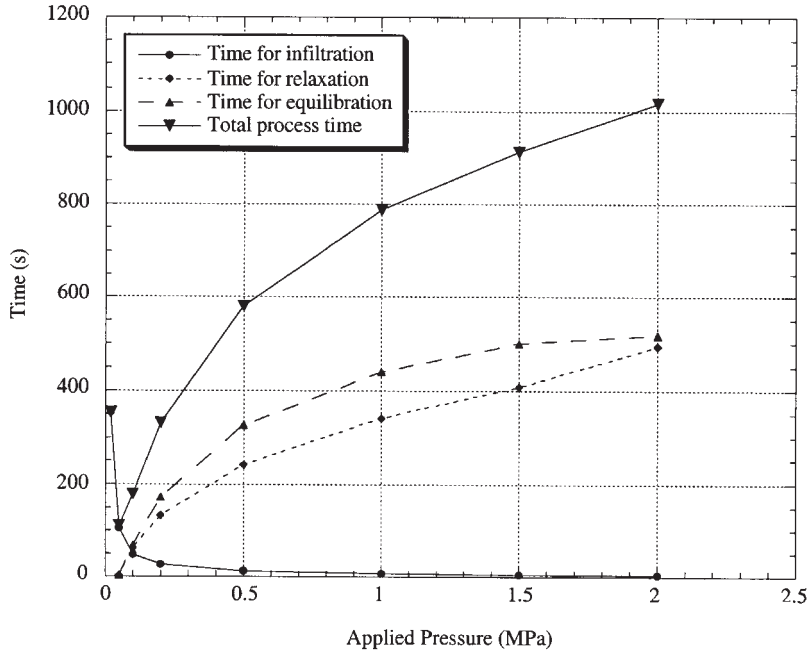

Figure 10. *Plot of the time for infiltration, time for relaxation, time for equilibration and total process time as a function of the applied pressure, for infiltration with a polymer viscosity of 250 Pa·s.*

which are then filled radially by the polymer. It then becomes important to consider the local pressure around the bundles within the thickness of the sample, as given in Figure 8, to predict a time for micro-impregnation which may, at low pressures, become larger than the total time for macro-impregnation and relaxation. An optimal value of applied pressure would then be defined based on the consideration of these two related time-scales.

CONCLUSION

A model is presented to simulate the kinetics of impregnation, and the evolution of the fiber volume fraction profile in liquid composite molding as the resin front progresses, as well as after the front has reached the end of the mold. The process was divided in three steps: (i) inflitration of the dry compressible preform, (ii) relaxation of the impregnated preform within the fluid after the infiltration front has reached the preform thickness, and (iii) possible equilibration of the fiber volume fraction to a higher level than the fully relaxed value if the final thickness of the sample is less than the thickness of the relaxed preform. Governing equations for the three steps are presented and solved with the relevant boundary conditions using numerical techniques. The analysis is then applied to an industrially relevant system, polypropylene and needled glass fiber mats used in the production of Glass Mat Thermoplastic blanks. The influences of fluid viscosity and applied pressure on the kinetics of the process and the resulting distribution of the reinforcement are quantified. It is shown that the time for preform relaxation in a viscous fluid may be much larger than that for full impregnation. As a result, an apparently well impregnated part may exhibit an inhomogeneous distribution of the reinforcement, in turn inducing a modification of the mechanical behavior and residual stress distribution. The present analysis can therefore be applied to provide guidelines for producing a homogenous composite, or inversely, to produce a graded structure in a controlled manner. The range of application covers many practical cases of composite impregnation, provided that the preform stress-strain curve, its permeability as a function of fiber volume fraction, and the necessary boundary conditions are known.

ACKNOWLEDGMENTS

This work is funded by the Fonds National de la Recherche Scientifique under contract no. 20-52625.97. The authors gratefully acknowledge Mr. H. J. Grajzgrund for taking part in this work during his studies and M. R. Törnqvist for stimulating discussions.

REFERENCES

1. Gutowski, T. G., T. Morigaki and Z. Cai. 1987. *J. of Comp. Mater.,* 21:172–188.

2. Toll, S. 1998. *Polymer Engineering and Science,* 38(8):1337–1350.
3. Dave, R. 1990. *J. of Comp. Mater.,* 24:23–41.
4. Tevino, L., K. Rupel, W. B. Young, M. J. Liou and L. J. Lee. 1991. *Polym. Comp.,* 12:20–29.
5. Lekakou, C., M. A. K. B. Johari and M. G. Bader. 1996. *Polymer Composites,* 17(5):666–672.
6. Gong, H. 1993. *Journal of Materials Processing Technology,* 37:363–371.
7. Toll, S. and Månson, J.-A.E., 1995. *J. Appl. Mech.,* 62, p. 223–226.
8. Gutowski, T. 1997. John Wiley and Sons, Inc. New York.
9. Michaud, V. J., J. L. Sommer, A. Mortensen. 1999. *Metal. and Mat. Trans.,* 30A, 2:471–482.
10. R. S. Dave, J. L. Kardos and M. P. Dudukovic. 1987. *Polym. Comp.,* 8, 29 and 123.
11. Saunders, R. A., C. Lekakou and M. G. Bader. 1999. *Composites Science and Technology,* 59:1483–1494.
12. Pillai, K. M., C. L. Tucker III and F. R. Phelan, Jr., 2000. *Composites: Part A,* 31:87–94.
13. Trochu, F. and X. T. Pham. 1999. Proceedings of the ICCM 12, Paris, France, Extended Abstracts, T. Massard and A. Vautrin eds, p. 720.
14. Sommer, J. and A. Mortensen. 1996. *J. Fluid Mech.,* 311:193–217.
15. Preziosi, L., 1996. *Surveys on Mathematics for Industry,* 6:167–214.
16. Preziosi, L., D. D. Joseph and G. S. Beavers. 1996. *International Journal of Multiphase Flow,* 22:1205–1222.
17. Ambrosi, D. and L. Preziosi. 1998. *Composites Part A,* 29A:5–18.
18. Antonelli, D. and A. Farina. 1999. *Composites Part A,* 30:1367–1385.
19. Crank, J. 1984. *Free and Moving Boundary Problems,* Clarendon Press, Oxford.
20. Murray, W. D. and F. Landis. 1959. *Journal of Heat Transfer,* Transactions of ASME, May, pp. 106–112.
21. Rappaz, M., M. Bellet and M. Deville. 1998. *Traité des Matériaux 10: Modélisation numérique en Science et Génie des Matériaux,* Presses Polytechniques et Universitaires Romandes.
22. Servais C., V. Michaud and J-A.E. Månson. 2000. *Polymer Composites*, in print.
23. Michaud V., R. Tornqvist and J-A.E. Månson. 2001. *J. Comp. Mat.,* 35(13):1174–1200.
24. Jang, J. and S. Han. 1999. *Composites Part A,* 30:1045–1053.